

Self-oscillation and Synchronisation Transitions in Elasto-Active Structures

Ellen Zheng,¹ Martin Brandenbourger,¹ Louis Robinet,¹ Peter Schall,¹ Edan Lerner,¹ and Corentin Coulais¹

¹*Institute of Physics, Universiteit van Amsterdam,
Science Park 904, 1098 XH Amsterdam, The Netherlands*

The interplay between activity and elasticity often found in active and living systems triggers a plethora of autonomous behaviors ranging from self-assembly and collective motion to actuation. Amongst these, spontaneous self-oscillations of mechanical structures is perhaps the simplest and most wide-spread type of non-equilibrium phenomenon. Yet, we lack experimental model systems to investigate the various dynamical phenomena that may appear. Here, we report self-oscillation and synchronization transitions in a centimeter-sized model system for one-dimensional elasto-active structures. By combining precision-desktop experiments of elastically coupled self-propelled particles with numerical simulations and analytical perturbative theory, we demonstrate that the dynamics of single chain follows a Hopf bifurcation. We show that this instability is controlled by a single non-dimensional elasto-active number that quantifies the interplay between activity and elasticity. Finally, we demonstrate that pairs of coupled elasto-active chains can undergo a synchronization transition: the oscillations phases of both chains lock when the coupling link is sufficiently stiff. Beyond the canonical case considered here, we anticipate our work to open avenues for the understanding and design of the self-organisation and response of active artificial and biological solids, e.g. in higher dimensions and for more intricate geometries.

Introduction. — Active matter systems exhibit exceptional collective, non-equilibrium properties resulting in anomalous dynamical and self-organizing behaviour that challenge conventional laws of statistical mechanics [1–10]. While researches have extensively focused on active fluids [2, 11]—which consist of collections of individual active particles with no particular geometry [12–16], active solids—which have a well defined reference state and hence exhibit elastic rather than viscous properties at long timescales [17–19]—have been much less studied, despite their potential in mimicking living matter and forming novel active materials [18–20].

Among all kinds of mechanical properties of active solids, self-oscillations are vital for biological systems such as flagella and cilia [21–23] and offer the prospect of autonomous mechanical behaviors in designer materials [18, 19, 24]. It is now well established that one-dimensional active chains exhibit flagellar motion: on the one hand, experimental studies have reported self-oscillatory behavior and synchronization in biological and colloidal systems [25–28]; on the other hand, theoretical and numerical studies have suggested that self-oscillations emerge from the competition between activity and elasticity [21–23, 26, 29–39]. Despite these advances, there are as of yet few model experimental platforms in which the predicted bifurcation scenarios that lead to self-oscillations and synchronization can be verified.

Here, to investigate dynamical transitions in elasto-active solids, we construct the experimental setup for a simplest form of active solids by elastically constraining centimeter-sized active particles in one-dimensional chains. By controlling the elasticity of such structures, we uncover the nature of the transition to self-oscillations and synchronisation. We find the transition to self-

oscillatory behavior is governed by a super-critical Hopf

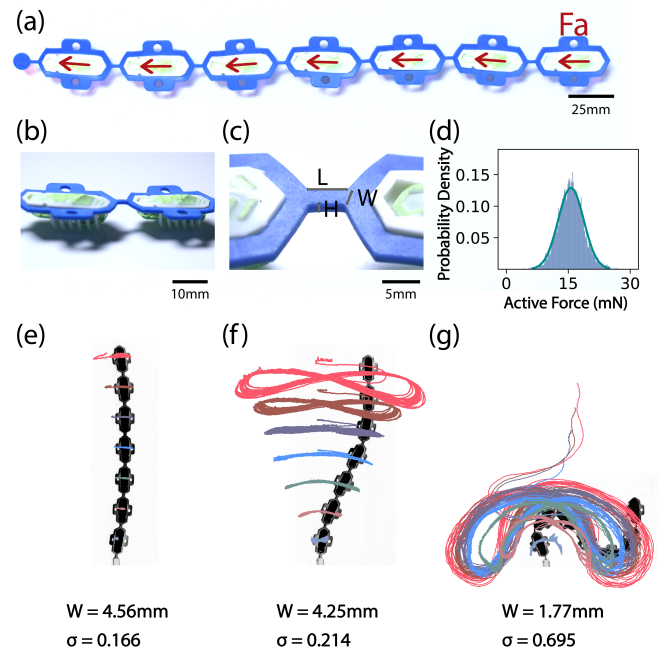


FIG. 1. Emergence of Self Oscillations in elasto-active chains (a) Configurations of 7 active particles connected by a flexible rubber chain (b) zoomed in details of two active particles unveiling the design of the microbot (c) a close-up of the linkage between each particle with width (W), thickness (H) and length (L). (d) Histogram of the active force measurements conducted at 0.05 mm/min. (e)-(f) Snapshots of the trajectories of the active particles showing the oscillations changed from self-amplified to overdamped with $W = 4.56\text{mm}$, 4.25mm and 1.77mm corresponding to elasto-active number $\sigma = 0.166$, 0.214 and 0.695 respectively.

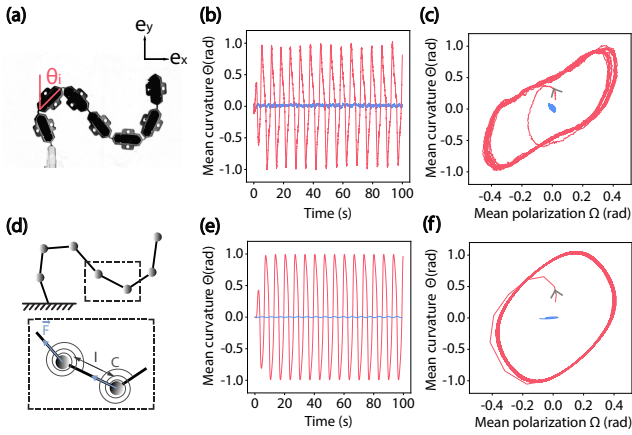


FIG. 2. **Characterisation of the dynamics of elasto-active chains.** (a) Snapshot of the elasto-active chain with $W=17.7\text{mm}$ during its self-oscillation. (b) Time series of the angle between the first and last particle (mean polarisation) was one of the parameters we chose to characterize the system, blue and orange represent the $\sigma = 0.695$ and $\sigma = 0.166$ chain respectively. With the average of tangential angles of the particles (mean curvature) being the other parameter, plotting mean polarisation (Θ) against mean curvature (Ω) gives (c) a hysteresis loop suggesting the system being time-irreversible. (d) Schematics of an elasto-active chain of 7 pendulums with active forces. (e)-(f) Simulation results at $\sigma=0.8$ showing good agreement with the experimental results

bifurcation and that the underlying mechanism is a non-linear feedback between the direction of the active forces and the nonlinear elastic deflections. We find that synchronization between two elasto-active chains is mediated by elastically driven alignment, in contrast with active fluids. Our work paves the way to a better understanding of elasto-active instabilities and provide design guidelines for autonomous behaviors in active solids.

Experimental design of active chains. — Our system consists of 7 5cm commercial self-propelled microbots (Hexbug Nano v2) elastically coupled by a laser-cut silicon rubber chain pinned at one end as shown in FIG.1(a). The self-propelling behaviour of the microbot is achieved by its soft rubber legs (see FIG.1(b)) interacting repetitively and impulsively with the ground [8, 40]. By tuning the width of the connection (W in FIG.1(c)), we are able to manipulate the stiffness of the chain. We measure the pulling force of a single microbot on a tensile test machine (Instron 5940 Series, load cell 5N with a resolution of 0.5mN) above a PET board, the results fluctuated rapidly due to the impulsive movement of the microbot and exhibited Gaussian distribution with a mean of 15.7mN and a standard deviation of 3.1mN (shown as FIG.1(d)). When constrained at zero velocity, the microbot exerts a force in the direction of its polarisation which is parallel to the chain's axis at rest and point in the same direction, towards the anchor point of the

chain. We placed the elasto-active chain on a black PET board and then tracked the motion of the active particles with a camera (Basler acA2040-90 μm , 4MPx, 60fps). The coupling force is provided by another laser-cut silicon rubber chain, connecting the two chains through plastic pins. The configurations of the elasto-active chains and coupling chains are further explained in Appendix A.

Transition to self-oscillations. — The chain with the largest width in between the active particles was slightly pushed off from the equilibrium and stayed at the same position without further significant movements as shown in FIG.1 (e). We then gradually reduced the width of the connections, at $W = 4.25 \pm 0.1\text{mm}$, the self-oscillation behaviour started to emerge (FIG.1 (f)) suggesting a competition between activity and elasticity: Active forces from active particles destabilise the elastic chain, which in turn, through deformation, re-orient the polarisation of the particle, ultimately leading to self-oscillation. The magnitude of the oscillations increases drastically (shown in FIG.1 (g)) with decreasing W thanks to the competition between buckling and active force. We chose to characterise the motion of the elasto-active chains in term of mean curvature $\Theta(t) := \sum_{i=1}^{N-1} \theta_{i+1}(t) - \theta_i(t)$, which amounts to the angle between the first and last particle on the chain $\Omega(t) = \theta_7 - \theta_1$ and in term of mean polarization $\Omega(t) := \sum_{i=1}^{N-1} \theta_i(t)$, where $\theta_i(t)$ is the instantaneous orientation of particle i w.r.t. the vertical axis (FIG.2 (a)). With such parameters, the dynamics of the oscillation can be visualized easily, as shown in FIG.2 (b), the red line depicts the mean curvature time series of the softest chain (see FIG.1 (g)) while the blue line corresponds to the chain with the widest connection, the scenario shown in FIG. 1(e). Plotting the time series of mean curvature against mean polarisation in FIG.2(c), we see an asymmetric hysteresis loop. Such limit cycle suggests the time-irreversible nature of the system [41].

Active pendulums model. — What is the origin of such transition? Inspired by the Ziegler destabilisation paradox in structural mechanics [42–45] and the existing numerical models of active filaments [46–49], we construct a discrete model, where we boil the complexity of the elastic interactions down to three-body bending forces between the particles and the complexity of the vibration-induced dynamics to viscous overdamped dynamics. The discrete model is based on a chain of seven pendulums (shown as FIG.2(d)) with one end fixed. The pendulums have a length ℓ and are connected to their neighbors via a torsional spring of torsional stiffness C . Each pendulum i is driven by a constant active force $\mathbf{F}_i^a = -F^a(\cos\theta_i\mathbf{e}_x + \sin\theta_i\mathbf{e}_y)$ exerted on its end and in the direction of the pendulum. We also introduce isotropic viscosity γ contributing to a dissipative force on the end of each pendulum that is only dependent on its velocity, and assume no inertia in the system. We then collected all the terms in $\delta\theta_i$ for each i according to Virtual-Work Theorem and constructed N nonlinear coupled ODEs

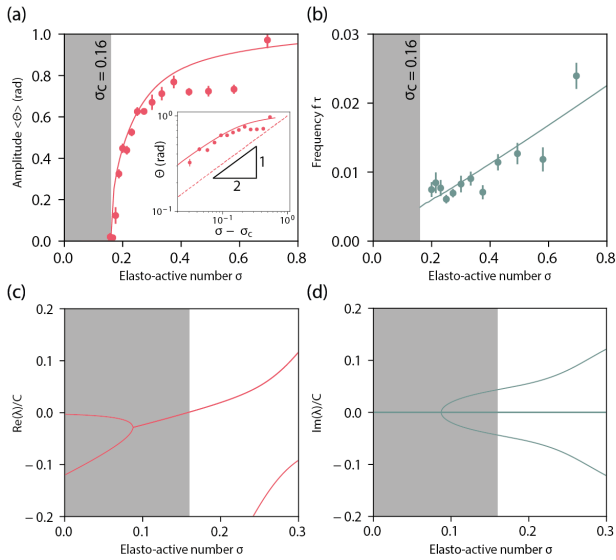


FIG. 3. **An active system featuring a Hopf bifurcation at $\sigma = 0.15$.** Simulation and experimental results showing the evolution of (a) amplitude and (b) frequency with increasing σ respectively for the chain with $N = 7$. The inset in (a) is a log-log plot demonstrating the power law between Θ and σ . (c) Real and imaginary (d) part of the eigenvalues of the Jacobian of Eqs. (1)-(2) vs. elasto-active number σ for a minimal chain with $N = 2$. In all panels, the gray area represents the stable region.

that describe the motion of the elasto-active chain (further details in Appendix B). where $\sigma = F^a \ell / C$ is the elasto-active parameter, and $\tau = \gamma \ell^2 / C$ a characteristic timescale. We estimate the torsional stiffness C from their geometry using beam theory (See Appendix A). From the average velocity of the robots when they are freely moving $v_{\mathbf{a}} = 0.025 \pm 0.005 \text{ m/s}$ and their average force when they are pinned $F_{\mathbf{a}} = 15.7 \pm 3.1 \text{ mN}$ (Fig. 1(d)), we estimate the damping coefficient $\gamma = F_{\mathbf{a}} / v_{\mathbf{a}} = 0.63 \pm 0.11 \text{ N.s/m}$. Using these parameters, we solve the system of ODEs numerically (See Appendix B) and find a good agreement with the experimental results, both for the time series of average polarisation (Fig. 2(e)). We observe an agreement between the experiments and the simulation in the trend of the hysteresis (Fig. 2(f)), here the differences are due to the energy loss in the experimental scenarios. This agreement shows that nonlinear geometry, torsional stiffness, active force and isotropic viscous dissipation are sufficient ingredients to successfully capture the essence of the self-oscillation phenomenon. Our elasto-active model is controlled by a single timescale τ and a single non-dimensional parameter σ , which will allow us to probe the nature of the transition to self-oscillations in the following.

Super-critical Hopf bifurcation. — We ran experiments and simulations over a wide range of the elasto-

active parameter σ , collected the time average of the amplitudes (Fig. 3 (a)) $\langle \Theta \rangle$ and the rescaled oscillation frequency $f \times \tau$ (Fig. 3 (b)) in the mean polarisation time series and plotted against elasto-active parameter σ . While for low values of σ , the chain remains straight without oscillations, we see that above a critical value $\sigma_c = 0.16 \pm 0.005$, the oscillation amplitude $\langle \Theta \rangle$ increases rapidly as $\langle \Theta \rangle \sim (\sigma - \sigma_c)^{0.5}$ (Fig. 3 (a-inset)), while the rescaled frequency increases linearly. To further elucidate the nature of the transition to self-oscillations, we carry out a linear stability analysis on the set of non-linear coupled equations (See Appendix B), and observe that at $\sigma = 0.15$, the real part of a pair of eigenvalues becomes positive, while the corresponding imaginary parts of these eigenvalues are equal and opposite and monotonically increase (Fig. 3(cd)). This transition is a hallmark of a Hopf-bifurcation. The exponent 0.5 in the experimental and numerical data suggests that this bifurcation is supercritical. To verify the nature of the bifurcation theoretically, we restrict our attention to two pendulums with $N = 2$, which is the simplest case where the model could exhibit the bifurcation. The time-evolution of such elasto-active chain is governed by the following equations

$$\tau \left(2\dot{\theta}_1 + \dot{\theta}_2 \cos(\theta_1 - \theta_2) \right) = \theta_2 - 2\theta_1 + \sigma \sin(\theta_1 - \theta_2) \quad (1)$$

$$\tau \left(\dot{\theta}_1 \cos(\theta_1 - \theta_2) + \dot{\theta}_2 \right) = \theta_1 - \theta_2. \quad (2)$$

In the Appendix B, we use a perturbative expansion and perform a few algebraic manipulations to demonstrate that Eqs. (1-2) can be mapped onto the Landau-Stuart equation

$$\frac{dz}{dt} = (i + \sigma - 3)z + \left(i \left(\frac{17}{4} - \sigma \right) - \left(\sigma - \frac{5}{2} \right) \right) |z|^2 z, \quad (3)$$

where z is the complex variable defined by $z := \theta_1 + i\sqrt{(\sigma - 2)/(4 - \sigma)}\theta_2$. Such equation is the canonical form of a supercritical Hopf-bifurcation. Many earlier works had observed experimentally or numerically self-oscillation phenomena [21, 25, 50] or theoretically proposed models with Hopf-bifurcations [23, 29, 30, 33, 49, 51]; here, we unambiguously demonstrate experimentally, numerically and theoretically in a single system of active chains that the supercritical Hopf bifurcation underlies the transition to self-oscillations and is primarily controlled by the elasto-active number σ .

Frequency entrainment synchronisation transition. — Our model system also allows us to explore synchronisation phenomena between two active chains (FIG.4 (a)-(d)). We demonstrate experimentally and numerically that an elastic coupling allows for a frequency entrainment synchronization transition. We selected two chains both with an elasto-active number $\sigma_1 = 0.8$ (the chain on the left hand side in FIG 4 (a)) and an elasto-active number $\sigma_2 = 0.6$ (the chain on the right hand side in FIG 4 (a)) and connected them via a coupling spring of variable

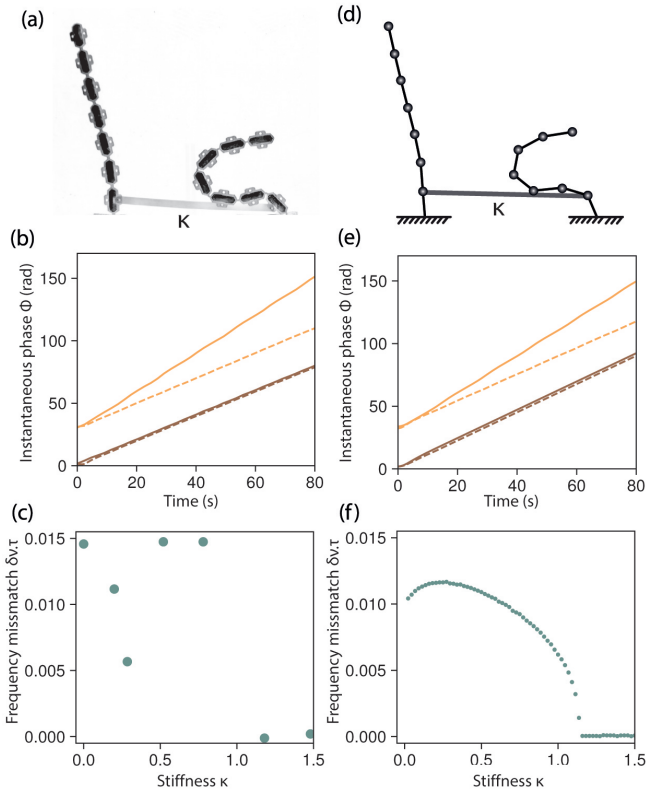


FIG. 4. **Synchronisation of two elasto-active chains with different elasticity coupled by the first particles only.** (a) Snapshot of a pair of elasto-active chains with different elasticity coupled by another stiff silicon rubber chain. (b) Evolution of the instantaneous phases Φ_1 (dashed lines) and Φ_2 (solid lines) of two elasto-active chains with coupling strength $K = 0.8$ (yellow lines) and $K = 1.2$ (brown lines). (c) Instantaneous frequency difference extracted from the instantaneous phase difference Ψ vs. rescaled coupling stiffness κ . (d) Schematics of the numerical model adding a coupling spring (K) to two previously established elasto-active chains. (e)-(f) Same data as (b)-(c) for the numerical simulations.

stiffness K . We also performed simulations over a range of stiffness K that contains what we have utilised in the experiments (FIG.4 (e)-(f)). The rescaled coupling stiffness is $\kappa := K\ell^2/C_1$ (where C_1 is the stiffness of the left chain). To analyze the synchronization transition, we first extracted the oscillation signals from both chains. We then calculated the instantaneous phases $\Phi_1(t)$ and $\Phi_2(t)$ (see Appendix A) of each timeseries (Fig. 4(b) and (e) for experiments and simulations respectively). For low coupling stiffness (yellow lines), both $\Phi_1(t)$ and $\Phi_2(t)$ increase linearly, but with different slope, which can be described as two chains oscillating with different frequencies. On the contrary, for large coupling stiffness (brown lines), both instantaneous phases $\Phi_1(t)$ and $\Phi_2(t)$ align on the lowest slope (i.e. both chains beat at the lowest frequency of the two). We performed experiments and

numerical simulations and measured the frequency mismatch $\delta\nu$ from the slope of the instantaneous phase difference $\Psi := \Phi_2(t) - \Phi_1(t)$ over a wide range of coupling stiffness and found that the synchronization transition occurs at the critical value $\kappa = 1.1$ (Fig. 4(c) and (f)).

To rationalize this finding, we show in Appendix B that the instantaneous phase difference $\Psi(t)$ between two flagella with $N = 2$ is

$$\frac{d\Psi}{dt} = d\nu - \frac{\varepsilon}{\cos\Psi_0} \sin(\Psi - \Psi_0), \quad (4)$$

where $d\nu$, ε and Ψ_0 are functions of the elasto-active number of each chain and of the coupling stiffness between the chains (See Appendix B for closed forms). This equation has been well studied before for the investigation of synchronization phenomena [52]. An analysis of this equation predicts synchronization for $|\varepsilon/\cos\psi_0| > |d\nu|$, with a square root singularity [52]. As we show in the appendix, this condition is met when the coupling stiffness exceeds the threshold value $\kappa_c = 11/(4\sqrt{6})\sqrt{(\sigma-3)|1-\rho|}$, where σ is the elasto-active number of the left chain and where ρ is ratio between the elasto-active number of the right chain over that of the left chain. This result thus demonstrates that the synchronization scenario of the two elasto-active chains corresponds to that of a classic nonisochronous synchronization, which is characterized by a constant phase shift in the synchronized region. In addition, the two chains will synchronize for lower coupling if they are closer to the bifurcation or when they have similar elasto-active numbers. In summary, we have captured experimentally, numerically and analytically the synchronization transition of two elastically coupled active chains.

Conclusion. — In conclusion, we have shown that elasto-active chains exhibit transitions to self-oscillations and synchronization. Our study establishes macroscopic active structures as a powerful tool to investigate dynamical and autonomous behavior of active solids and living matter. We anticipate the study of more intricate geometries, higher dimensions as well as non-reciprocal phenomena to be fascinating future research directions.

Acknowledgments. — We thank D. Giesen, S. Koot and all the staff members from the Technology Centre of University of Amsterdam for their outstanding technical support. We acknowledge K. Sekimoto, A. Deblais, D. Tam and M. Jalaal for insightful discussions. We acknowledge funding from the Netherlands Organization for Scientific Research through support from the NWO (Vidi grant no. 680-47-554/3259) and from the European Research Council Starting Grant No. ERC-StG-Coulais-852587-Extr3Me (C.C.).

[1] Suropriya Saha, Ramin Golestanian, and Sriram Ramaswamy, “Clusters, asters, and collective oscillations in

- chemotactic colloids,” *Phys. Rev. E* **89**, 062316 (2014).
- [2] M. C. Marchetti, J. F. Joanny, S. Ramaswamy, T. B. Liverpool, J. Prost, Madan Rao, and R. Aditi Simha, “Hydrodynamics of soft active matter,” *Rev. Mod. Phys.* **85**, 1143–1189 (2013).
 - [3] Sriram Ramaswamy, “Active matter,” *Journal of Statistical Mechanics: Theory and Experiment* **2017**, 054002 (2017).
 - [4] Clemens Bechinger, Roberto Di Leonardo, Hartmut Löwen, Charles Reichardt, Giorgio Volpe, and Giovanni Volpe, “Active particles in complex and crowded environments,” *Rev. Mod. Phys.* **88**, 045006 (2016).
 - [5] J. Deseigne, O. Dauchot, and H. Chate, “Collective motion of vibrated polar disks,” *Phys Rev Lett* **105**, 098001 (2010).
 - [6] C. A. Weber, T. Hanke, J. Deseigne, S. Léonard, O. Dauchot, E. Frey, and H. Chaté, “Long-range ordering of vibrated polar disks,” *Phys. Rev. Lett.* **110**, 208001 (2013).
 - [7] Antoine Bricard, Jean-Baptiste Caussin, Nicolas Desreumaux, Olivier Dauchot, and Denis Bartolo, “Emergence of macroscopic directed motion in populations of motile colloids,” *Nature* **503**, 95 (2013).
 - [8] O. Dauchot and V. Demery, “Dynamics of a self-propelled particle in a harmonic trap,” *Phys Rev Lett* **122**, 068002 (2019).
 - [9] Tamás Vicsek and Anna Zafeiris, “Collective motion,” *Physics Reports* **517**, 71 – 140 (2012), collective motion.
 - [10] Aparna Baskaran and M Cristina Marchetti, “Statistical mechanics and hydrodynamics of bacterial suspensions,” *Proceedings of the National Academy of Sciences* **106**, 15567–15572 (2009).
 - [11] David Saintillan and Michael J Shelley, “Active suspensions and their nonlinear models,” *Comptes Rendus Physique* **14**, 497–517 (2013).
 - [12] Peter Reimann, “Brownian motors: noisy transport far from equilibrium,” *Physics Reports* **361**, 57 – 265 (2002).
 - [13] Walter F Paxton, Kevin C Kistler, Christine C Olmeda, Ayusman Sen, Sarah K St. Angelo, Yanyan Cao, Thomas E Mallouk, Paul E Lammert, and Vincent H Crespi, “Catalytic nanomotors: autonomous movement of striped nanorods,” *Journal of the American Chemical Society* **126**, 13424–13431 (2004).
 - [14] Jonathan R Howse, Richard AL Jones, Anthony J Ryan, Tim Gough, Reza Vafabakhsh, and Ramin Golestanian, “Self-motile colloidal particles: from directed propulsion to random walk,” *Physical review letters* **99**, 048102 (2007).
 - [15] Eric Lauga and Thomas R Powers, “The hydrodynamics of swimming microorganisms,” *Reports on Progress in Physics* **72**, 096601 (2009).
 - [16] WCK Poon, “From clarkia to escherichia and janus: The physics of natural and synthetic active colloids,” *Proc. Int. Sch. Phys. Enrico Fermi* **184**, 317–386 (2013).
 - [17] Rhoda J Hawkins and Tanniemola B Liverpool, “Stress reorganization and response in active solids,” *Physical review letters* **113**, 028102 (2014).
 - [18] M. Brandenbourger, X. Locsin, E. Lerner, and C. Coullais, “Non-reciprocal robotic metamaterials,” *Nat Commun* **10**, 4608 (2019).
 - [19] Colin Scheibner, Anton Souslov, Debarghya Banerjee, Piotr Surówka, William T. M. Irvine, and Vincenzo Vitelli, “Odd elasticity,” *Nat. Phys.* **16**, 475–480 (2020).
 - [20] Y. Ozkan-Aydin, D. I. Goldman, and M. S. Bhamla, “Collective dynamics in entangled worm and robot blobs,” *Proc Natl Acad Sci U S A* **118** (2021), 10.1073/pnas.2010542118.
 - [21] KE Machin, “Wave propagation along flagella,” *Journal of Experimental Biology* **35**, 796–806 (1958).
 - [22] Charles J Brokaw, “Molecular mechanism for oscillation in flagella and muscle,” *Proceedings of the National Academy of Sciences* **72**, 3102–3106 (1975).
 - [23] Sébastien Camalet, Frank Jülicher, and Jacques Prost, “Self-organized beating and swimming of internally driven filaments,” *Physical review letters* **82**, 1590 (1999).
 - [24] F. G. Woodhouse, H. Ronellenfitsch, and J. Dunkel, “Autonomous actuation of zero modes in mechanical networks far from equilibrium,” *Phys Rev Lett* **121**, 178001 (2018).
 - [25] Daiki Nishiguchi, Junichiro Iwasawa, Hong-Ren Jiang, and Masaki Sano, “Flagellar dynamics of chains of active janus particles fueled by an ac electric field,” *New Journal of Physics* **20**, 015002 (2018).
 - [26] Kirsty Y Wan, Kyriacos C Leptos, and Raymond E Goldstein, “Lag, lock, sync, slip: the many ‘phases’ of coupled flagella,” *Journal of the Royal Society Interface* **11**, 20131160 (2014).
 - [27] Douglas R Brumley, Kirsty Y Wan, Marco Polin, and Raymond E Goldstein, “Flagellar synchronization through direct hydrodynamic interactions,” *Elife* **3**, e02750 (2014).
 - [28] Raymond E Goldstein, Marco Polin, and Idan Tuval, “Emergence of synchronized beating during the re-growth of eukaryotic flagella,” *Physical Review Letters* **107**, 148103 (2011).
 - [29] A Hilfinger and F Jülicher, “The chirality of ciliary beats,” *Physical biology* **5**, 016003 (2008).
 - [30] Andreas Hilfinger, Amit K Chattopadhyay, and Frank Jülicher, “Nonlinear dynamics of cilia and flagella,” *Physical Review E* **79**, 051918 (2009).
 - [31] Henry C Fu, Charles W Wolgemuth, and Thomas R Powers, “Beating patterns of filaments in viscoelastic fluids,” *Physical Review E* **78**, 041913 (2008).
 - [32] Jannes Gladrow, Chase P Broedersz, and Christoph F Schmidt, “Nonequilibrium dynamics of probe filaments in actin-myosin networks,” *Physical Review E* **96**, 022408 (2017).
 - [33] Raghunath Chelakkot, Arvind Gopinath, Lakshminarayanan Mahadevan, and Michael F Hagan, “Flagellar dynamics of a connected chain of active, polar, brownian particles,” *Journal of The Royal Society Interface* **11**, 20130884 (2014).
 - [34] Greta Quaranta, Marie-Eve Aubin-Tam, and Daniel Tam, “Hydrodynamics versus intracellular coupling in the synchronization of eukaryotic flagella,” *Physical review letters* **115**, 238101 (2015).
 - [35] Kirsty Y Wan and Raymond E Goldstein, “Coordinated beating of algal flagella is mediated by basal coupling,” *Proceedings of the National Academy of Sciences* **113**, E2784–E2793 (2016).
 - [36] Thomas Niedermayer, Bruno Eckhardt, and Peter Lenz, “Synchronization, phase locking, and metachronal wave formation in ciliary chains,” *Chaos: An Interdisciplinary Journal of Nonlinear Science* **18**, 037128 (2008).
 - [37] Boris Guirao and Jean-François Joanny, “Spontaneous creation of macroscopic flow and metachronal waves in an array of cilia,” *Biophysical journal* **92**, 1900–1917 (2007).
 - [38] Rachel R Bennett and Ramin Golestanian, “Emergent

- run-and-tumble behavior in a simple model of chlamydomonas with intrinsic noise,” *Physical review letters* **110**, 148102 (2013).
- [39] Andrej Vilfan and Frank Jülicher, “Hydrodynamic flow patterns and synchronization of beating cilia,” *Physical review letters* **96**, 058102 (2006).
- [40] David L. Christensen, Srinivasan A. Suresh, Katie Hahm, and Mark R. Cutkosky, “Let’s All Pull Together: Principles for Sharing Large Loads in Microrobot Teams,” *IEEE Robotics and Automation Letters* **1**, 1089–1096 (2016).
- [41] C. Battle, C. P. Broedersz, N. Fakhri, V. F. Geyer, J. Howard, C. F. Schmidt, and F. C. MacKintosh, “Broken detailed balance at mesoscopic scales in active biological systems,” *Science* **352**, 604–7 (2016).
- [42] F. Bosi, D. Misseroni, F. Dal Corso, S. Neukirch, and D. Bigoni, “Asymptotic self-restabilization of a continuous elastic structure,” *Physical Review E* **94**, 1–10 (2016).
- [43] Peter Hagedorn, “on the Destabilizing Effect of Non-Linear Damping in Non-Conservative Systems With Follower Forces,” **5**, 341–358 (1970).
- [44] Davide Bigoni and Giovanni Noselli, “Experimental evidence of flutter and divergence instabilities induced by dry friction,” *Journal of the Mechanics and Physics of Solids* **59**, 2208–2226 (2011).
- [45] H. Ziegler, “Die Stabilitätskriterien der Elastomechanik,” *Ingenieur-Archiv* **20**, 49–56 (1952).
- [46] Zeno Farkas, Imre Derényi, and Tomas Vicsek, “Dynamics of Actin Filaments in Motility Assays,” *Structure and Dynamics of Confined Polymers* , 327–332 (2002).
- [47] Rolf E. Isele-Holder, Jens Elgeti, and Gerhard Gompper, “Self-propelled worm-like filaments: spontaneous spiral formation, structure, and dynamics,” *Soft Matter* **11**, 7181–7190 (2015), arXiv:1508.01418.
- [48] Roland G. Winkler, Jens Elgeti, and Gerhard Gompper, “Active polymers — Emergent conformational and dynamical properties: A brief review,” *Journal of the Physical Society of Japan* **86**, 1–14 (2017).
- [49] Ken Sekimoto, Naoki Mori, Katsuhisa Tawada, and Yoko Y. Toyoshima, “Symmetry breaking instabilities of an in vitro biological system,” *Physical Review Letters* **75**, 172–175 (1995).
- [50] Chien-Jung Lo, Yoshiyuki Sowa, Teuta Pilizota, and Richard M Berry, “Mechanism and kinetics of a sodium-driven bacterial flagellar motor,” *Proceedings of the National Academy of Sciences* **110**, E2544–E2551 (2013).
- [51] S Gonzalez and R Soto, “Active colloidal chains with cilia-and flagella-like motion,” *New Journal of Physics* **20**, 053014 (2018).
- [52] Arkady Pikovsky, Michael Rosenblum, and Jürgen Kurths, “Synchronization: a universal concept in nonlinear science,” (2002).
- [53] Warren Clarence Young, Richard Gordon Budynas, Ali M Sadegh, *et al.*, *Roark’s formulas for stress and strain*, Vol. 7 (McGraw-Hill New York, 2002).
- [54] (2006).
- [55] J. Guckenheimer and P. Holmes, *Nonlinear Oscillations, Dynamical Systems, and Bifurcations of Vector Fields*, Applied Mathematical Sciences (Springer, 1983).

Appendix A. Experimental methods

Construction of one-dimensional elasto-active chain

Our elasto-active chain is simply constructed by 7 active units in a laser-cut silicon rubber chain. We fix one end of the chain with a clamp mechanically fixed by silicon glue on a 1.5mx1.5m black PET board. A camera (Basler acA2040-90 μ m) was mounted on an aluminium profile above the chain to track its motion.

active units - HEXBUG nano[®] (random color) plays the role of active particle in our system. It is a self-propelled microbot powered by a tiny motor (with AG13/LR44 1.5V button battery) and 12 rubber legs as shown in Fig. 1.(b).

Laser-cut rubber chain - We first constructed the models of the rubber chains using Autodesk Inventor[®] then printed the model with Universal Laser PLS6.150D. Width of the connection in the model increased from 2mm to 5mm with a 0.2mm step, the rest of the geometries unchanged. The 'ears' on the side of the constraining units were designed for the convenience of connecting two single chains together. The circular end was made to ease the fixation to the clamp. Real geometries of the chains printed from the laser cutter differs slightly with the geometries in the model, they were measured again using vernier caliper. The flexibility of the silicone rubber chain brought negligible errors in geometry measurements, the real thickness was set to be the value at which the chain can not be clipped by the caliper anymore.

Realisation of the coupled elasto-active chains

Taking two elasto-active chains with $W = 2\text{mm}$ and 2.8mm respectively, we connected the two of them with different coupling chains. The coupling chain was fixed onto the 'ears' of the elasto-active chains with plastic pins, the elasto-active chains themselves were fixed by the clamps in the same way as the singular chains. The highest stiffness was provided by a simple rubber chain (380mmx15mm), we then tuned the stiffness by adding triangular teeth to the simple geometry. The coupling chain with 1 teeth possessed the lowest stiffness while adding more teeth to it slightly increased the stiffness. Schematics of the chains can be found in the supplementary materials.

Calibration and measurements

Torsional Stiffness - As mentioned in the main paragraph, we measured the Young's modulus of the silicon rubber with Instron 5940 Series at a strain rate of 0.05 mm/min. Torsional stiffness (C) of the connections shown in FIG.1(c) was calculated [53] with:

$$C = \frac{GJ}{L} \quad (\text{A1})$$

where G was taken as the Young's modulus (0.239MPa) and J is the torsional constant that was determined with:

$$J = w^3h\left(\frac{16}{3} - 3.36\frac{2}{h}\left(1 - \frac{w^4}{12h^4}\right)\right) \quad (\text{A2})$$

where h and w was half the value of H and W shown in FIG.1(c)

Tracking of Motion - Motion of the active chains was recorded by the camera (Basler acA2040-90 μ m) at a frame rate of 60fps and resolution of 4Mpx. The images were binarized and eroded, we then detected and tracked the active units using the opencv module under Python.

Instantaneous phase - The exact oscillation frequency of the two coupled active-chains was obtained by computing their instantaneous phase over time. We expressed the signal $s(t)$ in its analytical form $s_a(t)$:

$$s_a(t) = s(t) + j\hat{s}(t) = s_m(t)e^{j\phi(t)}, \quad (\text{A3})$$

where $\hat{s}(t) \triangleq \mathcal{H}[s(t)]$ is the Hilbert transform of the signal and $s_m(t)$ is the instantaneous amplitude of the envelope. The instantaneous phase of the signal corresponds to $\phi(t) \triangleq \arg[s_a(t)]$ and is plotted in Fig. 4b&c in the main text. The instantaneous frequency was calculated via a linear regression on the instantaneous phase. The Fig 4c&e show the mismatch between the two instantaneous frequencies of the chains.

Appendix B. Theoretical Models

Derivation of equations of motion

Single elasto-active chain

We aim to describe the active chain shown in Fig. 1a by a model of a elasto-active chain of N pendula, with follower forces. The potential energy is

$$U = \frac{C}{2}\theta_1^2 + \frac{C}{2}\sum_{i=1}^{N-1}(\theta_i - \theta_{i+1})^2, \quad (\text{A4})$$

where C is the torsional stiffness of the links between each pendulum and θ_i the angle of pendulum i with respect to the \mathbf{e}_x axis in Fig. 1(d). Upon an infinitesimal variation of the internal degrees of freedoms, the change in potential energy is $\delta U = \sum_{i=1}^N (\partial U / \partial \theta_i) \delta \theta_i$ that yields

$$\delta U = C(2\theta_1 - \theta_2)\delta\theta_1 + C(2\theta_2 - \theta_1\theta_3)\delta\theta_2 + \dots + C(2\theta_{N-1} - \theta_{N-2}\theta_N)\delta\theta_{N-1} + C(\theta_N - \theta_{N-1})\delta\theta_N. \quad (\text{A5})$$

In addition, each particle i located at the endpoint of each pendulum undergoes an active force $\mathbf{F}_i^a = -F^a(\cos\theta_i\mathbf{e}_x + \sin\theta_i\mathbf{e}_y)$, aligned with the pendulum i and a dissipative force, which we assume is viscous $-\gamma(\dot{x}_i\mathbf{e}_x + \dot{y}_i\mathbf{e}_y)$. γ is the damping coefficient, F the follower force exerted on each pendulum, ℓ the length of each pendulum and x_i (y_i) the horizontal (vertical) displacement of the end point of pendulum i . $\dot{}$ denote the time derivative. Therefore, the work of these non-conservative forces upon infinitesimal variation of the internal degrees of freedoms $\{\delta x_1, \delta x_2, \dots, \delta x_N, \delta y_1, \delta y_2, \dots, \delta y_N\}$ of the system reads

$$\delta W = -\gamma \sum_{i=1}^N (\dot{x}_i \delta x_i + \dot{y}_i \delta y_i) - F^a \sum_{i=1}^N (\cos\theta_i \delta x_i + \sin\theta_i \delta y_i), \quad (\text{A6})$$

Thanks to the geometrical relations $x_i = \ell \sum_{j=1}^i \cos\theta_j$ and $y_i = \ell \sum_{j=1}^i \sin\theta_j$, we can substitute $\delta x_i = \ell \sum_{j=1}^i -\sin\theta_j \delta\theta_j$, $\delta y_i = \ell \sum_{j=1}^i \cos\theta_j \delta\theta_j$, $\dot{x}_i = \ell \sum_{j=1}^i -\sin\theta_j \dot{\theta}_j$, $\dot{y}_i = \ell \sum_{j=1}^i \cos\theta_j \dot{\theta}_j$, and Eq. (A6) can be rewritten as a function of the angles

$$\delta W = -\gamma \ell^2 \sum_{i=1}^N \sum_{j=1}^i \sum_{k=1}^i \left(\cos(\theta_j - \theta_k) \dot{\theta}_j \delta\theta_k \right) - F^a \ell \sum_{i=1}^N \sum_{j=1}^i (\sin(\theta_i - \theta_j) \delta\theta_j). \quad (\text{A7})$$

According to the Virtual-Work Theorem, at mechanical equilibrium, the work of external forces δW (Eq. (A7)) is equal to the change of potential energy δU (Eq. (A5)). Collecting all the terms in $\delta\theta_i$ for each i , With dimensionless parameters: $\sigma = F^a \ell / C$ and $\tau = \gamma \ell^2 / C$, we find N nonlinear coupled ordinary differential equations that describe the motion of the elasto-active chain.

$$0 = 2\theta_1 - \theta_2 - \sigma \sum_{j=1}^N \sin(\theta_1 - \theta_j) + \tau \left(N\dot{\theta}_1 + \sum_{j=2}^N \dot{\theta}_j \cos(\theta_1 - \theta_j) \right) \text{ for } i = 1 \quad (\text{A8})$$

$$0 = 2\theta_i - \theta_{i-1} - \theta_{i+1} - \sigma \sum_{j=i}^N \sin(\theta_i - \theta_j) + \tau \left((N-i+1) \sum_{j=1}^i \dot{\theta}_j \cos(\theta_i - \theta_j) + \sum_{j=i+1}^N (N-j+1) \dot{\theta}_j \cos(\theta_i - \theta_j) \right) \text{ for } i \in [2, N-1] \quad (\text{A9})$$

$$0 = \theta_N - \theta_{N-1} + \tau \sum_{j=i}^N \dot{\theta}_j \cos(\theta_N - \theta_j) \text{ for } i = N, \quad (\text{A10})$$

which are the equations that we solve numerically in Figs. 2 and 3 or the Main Text.

Coupled elasto-active chains

For a pair of coupled elasto-active chains with different elasticity, we took the work done by the dissipative force F_d and the active force F_a as a sum of these values of both chains. The resulting δW is thus:

$$\begin{aligned} \delta W = & -\gamma l^2 \left(\sum_{i=1}^N \left(\sum_{j=1}^i \left(\sum_{k=1}^i \delta \theta_k \dot{\theta}_j \cos(\theta_j - \theta_k) \right) \right) \right) + \sum_{i=1}^N \left(\sum_{j=1}^i \left(\sum_{k=1}^i \delta \phi_k \dot{\phi}_j \cos(\phi_j - \phi_k) \right) \right) \\ & - F^a \ell \left(\sum_{i=1}^N \left(\sum_{j=1}^i \delta \theta_j \sin(\theta_i - \theta_j) \right) + \sum_{i=1}^N \left(\sum_{j=1}^i \delta \phi_j \sin(\phi_i - \phi_j) \right) \right), \end{aligned} \quad (\text{A11})$$

where θ_i and ϕ_i depict the angle between each particle and the horizontal axis of individual chains. We then added the effect of the coupling force to the sum of δU of both chains and rendered:

$$\begin{aligned} \delta U = & \theta_1 (\delta \theta_1 (C_1 + K) - \delta \phi_1 K) + \phi_1 (\delta \phi_1 (C_2 + K) - \delta \theta_1 K) + C_1 \sum_{i=2}^N \delta \theta_i (\theta_i - \theta_{i-1}) + C_1 \sum_{i=1}^{N-1} \delta \theta_i (\theta_i - \theta_{i+1}) \\ & + C_2 \sum_{i=2}^N \delta \phi_i (\phi_i - \phi_{i-1}) + C_2 \sum_{i=1}^{N-1} \delta \phi_i (\phi_i - \phi_{i+1}), \end{aligned} \quad (\text{A12})$$

where C_1 and C_2 are the torsional spring constant in each chain and K is the stiffness of the coupling chain. We introduced the following dimensionless parameters

$$\rho = \frac{C_2}{C_1}, \quad \kappa = \frac{K \ell^2}{C_1}, \quad \sigma = \frac{F^a \ell}{C_1} \quad \text{and} \quad \tau = \frac{\gamma l^2}{C_1}, \quad (\text{A13})$$

which allowed to express the coupled ordinary differential equations as follows

$$\begin{aligned} 0 = & (2 + \kappa) \theta_1 - \theta_2 - \kappa \phi_1 - \sigma \sum_{j=1}^N \sin(\theta_1 - \theta_j) + \tau \left(N \dot{\theta}_1 + \sum_{j=2}^N (N - j + 1) \dot{\theta}_j \cos(\theta_1 - \theta_j) \right); \\ 0 = & (2\rho + \kappa) \phi_1 - \rho \phi_2 - \kappa \theta_1 - \sigma \sum_{j=1}^N \sin(\phi_1 - \phi_j) + \\ & \tau \left(N \dot{\phi}_1 + \sum_{j=2}^N (N - j + 1) \dot{\phi}_j \cos(\phi_1 - \phi_j) \right) \quad \text{for } i = 1 \end{aligned} \quad (\text{A14})$$

$$\begin{aligned} 0 = & 2\theta_i - \theta_{i-1} - \theta_{i+1} - \sigma_1 \sum_{j=i}^N \sin(\theta_i - \theta_j) + \\ & \tau \left((N - i + 1) \sum_{j=1}^i \dot{\theta}_j \cos(\theta_i - \theta_j) + \sum_{j=i+1}^N (N - j + 1) \dot{\theta}_j \cos(\theta_i - \theta_j) \right); \\ 0 = & \rho(2\phi_i - \phi_{i-1} - \phi_{i+1}) - \sigma \sum_{j=i}^N \sin(\phi_i - \phi_j) + \\ & \tau \left((N - i + 1) \sum_{j=1}^i \dot{\phi}_j \cos(\phi_i - \phi_j) + \sum_{j=i+1}^N (N - j + 1) \dot{\phi}_j \cos(\phi_i - \phi_j) \right) \quad \text{for } i \in [2, N - 1] \end{aligned} \quad (\text{A15})$$

$$\begin{aligned} 0 = & \theta_N - \theta_{N-1} + \tau \sum_{j=i}^N \dot{\theta}_j \cos(\theta_N - \theta_j); \\ 0 = & \rho(\phi_N - \phi_{N-1}) + \tau \sum_{j=i}^N \dot{\phi}_j \cos(\phi_N - \phi_j) \quad \text{for } i = N. \end{aligned} \quad (\text{A16})$$

We solved numerically these coupled non-linear equations in Fig. 4 of the Main Text. Below in the Section ‘‘Synchronization of two coupled elasto-active chains’’, we considered the case $N = 2$ and performed a perturbative expansion to map these ODEs onto an equation that describes the time evolution of the instantaneous phase difference between two elasto-active chains.

Linear limits

Eqs. (A8)-(A10) are impossible to solve explicitly in their full generality, but we can obtain some information about the behavior of the system by considering its linearisation close to the limit where all the angle are zero.

$$0 = 2\theta_1 - \theta_2 - \frac{Fa^2}{C} \sum_{j=1}^N (\theta_1 - \theta_j) + \frac{\gamma a^2}{C} \left(N\dot{\theta}_1 + \sum_{j=2}^N \dot{\theta}_j \right) \quad (\text{A17})$$

$$0 = 2\theta_i - \theta_{i-1} - \theta_{i+1} - \frac{Fa^2}{C} \sum_{j=i}^N (\theta_i - \theta_j) + \frac{\gamma a^2}{C} \left((N-i+1) \sum_{j=1}^i \dot{\theta}_j + \sum_{j=i+1}^N (N-j+1) \dot{\theta}_j \right) \text{ for } i \in [2, N-1] \quad (\text{A18})$$

$$0 = \theta_N - \theta_{N-1} + \frac{\gamma a^2}{C} \sum_{j=i}^N \dot{\theta}_j. \quad (\text{A19})$$

The stability of the system can be investigated by injecting the following ansatz

$$\underbrace{\begin{bmatrix} \theta_1 \\ \theta_2 \\ \vdots \\ \vdots \\ \theta_i \\ \vdots \\ \theta_N \end{bmatrix}}_{1 \times N} = \underbrace{\begin{bmatrix} \theta_1^0 \\ \theta_2^0 \\ \vdots \\ \vdots \\ \theta_i^0 \\ \vdots \\ \theta_N^0 \end{bmatrix}}_{1 \times N} \exp(\lambda t), \quad (\text{A20})$$

in Eqs. (A17)-(A19) and requiring that the determinant of such system of equation to be zero, which which can be rewritten in the following matrix form:

$$\underbrace{\begin{bmatrix} 0 \\ 0 \\ \vdots \\ \vdots \\ 0 \\ \vdots \\ \vdots \\ 0 \end{bmatrix}}_{1 \times N} = \underbrace{\begin{bmatrix} 2 & b - k_2 & 0 & \cdots & \cdots & \cdots & \cdots & 0 \\ -k_2 & 2k_2 + \lambda & -k_2 & 0 & \cdots & \cdots & \cdots & 0 \\ 0 & -k_2 & 2k_2 + \lambda & -k_2 & 0 & \cdots & \cdots & 0 \\ \vdots & \vdots & \ddots & \ddots & \ddots & \ddots & \vdots & \vdots \\ \vdots & \vdots & \vdots & \vdots & -k_2 & 2k_2 + \lambda & -k_2 & 0 \\ \vdots & \vdots & \cdots & \cdots & 0 & -k_2 & 2k_2 + \lambda & -k_2 \\ 0 & 0 & \cdots & \cdots & \cdots & 0 & -k_2 & k_2 \end{bmatrix}}_{N \times N} \underbrace{\begin{bmatrix} \theta_1 \\ \theta_2 \\ \vdots \\ \vdots \\ \theta_i \\ \vdots \\ \theta_N \end{bmatrix}}_{1 \times N}. \quad (\text{A21})$$

In Fig. 3 of the Main Text, we plot the real and imaginary parts of λ to discuss the stability of the elasto-active chain and the nature of the bifurcation.

Derivation of the canonical form of the Hopf bifurcation

In this section, we focus on the minimal case of an elasto-active chain with two active particles $N = 2$, see Eqs. (1)-(2) of the Main Text and show that they can be mapped onto the Landau-Stuart equation, which is the normal form

of a Hopf-bifurcation. First, we rewrite these equations as

$$\dot{\theta}_1 = \frac{-\sigma \sin(\theta_1 - \theta_2) + (\theta_1 - \theta_2) \cos(\theta_1 - \theta_2) + 2\theta_1 - \theta_2}{\tau (\cos^2(\theta_1 - \theta_2) - 2)} \quad (\text{A22})$$

$$\dot{\theta}_2 = \frac{\sigma \sin(2\theta_1 - 2\theta_2) + 2(\theta_2 - 2\theta_1) \cos(\theta_1 - \theta_2) - 4\theta_1 + 4\theta_2}{\tau (\cos(2\theta_1 - 2\theta_2) - 3)} \quad (\text{A23})$$

We find that the Jacobian of this system of equation admits conjuguate eigenvalues, whose real part crosses zero at $\rho = 3$. We therefore introduce the variable $\mu := \rho - 3$ and we will focus in the following on the transition point at $\mu = 0$. In order to map onto the canonical form, we define the variable $z := a\theta_1 + ib\theta_2$, where a and b are arbitrary real numbers. To find which values of a and b allow up to find the canonical form, we first linearize the equation. We find

$$\tau \dot{z} = \frac{(b + ia)(a(\mu + 1) - ib(\mu - 1))}{2ab} z - \frac{i(a^2(\mu + 1) + b^2(\mu - 1))}{2ab} z^* + \mathcal{O}(z^2). \quad (\text{A24})$$

The linear term of the canonical form of the Hopf-bifurcation has no z^* term, therefore we choose a and b such that this term cancels out, that is $a = 1$ and $b/a = \sqrt{(1 + \mu)/(1 - \mu)}$. We now use these values and rewrite \dot{z} up to cubic order in z and linearize the expression in μ

$$\begin{aligned} \tau \dot{z} = & (i + \mu)z + \frac{(10 + 4i)\mu + (-1 + 8i)}{8} |z|^2 z \\ & + \frac{-(1 - 2i)(16\mu + 8(2 - 3i))}{8} |z|^2 z^* + \frac{(6 - 9i) - (24 + 14i)\mu}{24} z^3 + \frac{(14 + 12i)\mu + (6 - 9i)}{24} z^{*3} \\ & + \mathcal{O}(z^4). \end{aligned} \quad (\text{A25})$$

Variable changes of the form $z = \tilde{z} + \alpha_{pq} \tilde{z}^p \tilde{z}^{*q}$, with $p \in [0, 3]$, $q \in [0, 3]$ and $p + q = 3$ can cancel out the cubic terms of Eq. (A25), except for $p = 2$ and $q = 1$, where the associated constraint diverges at the bifurcation $\mu = 0$ [54]. Thereby, we obtain the final equation

$$\tau \dot{z} = (i + \mu)z + \left(-1 - \frac{\mu}{2} + i \left(-\frac{1}{8} + \frac{5}{4}\mu \right) \right) |z|^2 z + \mathcal{O}(z^4). \quad (\text{A26})$$

The prefactor of the cubic term is called the first Lyapunov coefficient and its real part is negative for small μ , therefore the Hopf bifurcation is supercritical [55], as discussed in the Main Text.

Synchronization of two coupled elasto-active chains

In this section, we investigate theoretically the nature of the synchronization transition observed in Fig. 4 of the Main Text. To this end, we focus on with the minimal case of two elastically coupled elasto-active chains. Following Eqs. (A14-A16), such elasto-active chains are described by the following set of ODEs:

$$\dot{\theta}_1 = -\frac{-\theta_1 (\cos(\theta_1 - \theta_2) + 2) + \sigma \sin(\theta_1 - \theta_2) + \theta_2 (\cos(\theta_1 - \theta_2) + 1) - \kappa(\theta_1 - \phi_1)}{\tau (\cos^2(\theta_1 - \theta_2) - 2)} \quad (\text{A27})$$

$$\dot{\theta}_2 = \frac{2 \cos(\theta_1 - \theta_2) (\theta_2 + \kappa\phi_1) - 2\theta_1 ((\kappa + 2) \cos(\theta_1 - \theta_2) + 2) + \sigma \sin(2(\theta_1 - \theta_2)) + 4\theta_2}{\tau (\cos(2(\theta_1 - \theta_2)) - 3)}, \quad (\text{A28})$$

$$\dot{\phi}_1 = -\frac{\theta_1 \kappa - \phi_1 (\kappa + \rho \cos(\phi_1 - \phi_2) + 2\rho) + \rho\phi_2 (\cos(\phi_1 - \phi_2) + 1) + \sigma \sin(\phi_1 - \phi_2)}{\tau (\cos^2(\phi_1 - \phi_2) - 2)} \quad (\text{A29})$$

$$\dot{\phi}_2 = \frac{-2 \cos(\phi_1 - \phi_2) (\phi_1 (\kappa + 2\rho) - \theta_1 \kappa) - 4\rho\phi_1 + 2\rho\phi_2 (\cos(\phi_1 - \phi_2) + 2) + \sigma \sin(2(\phi_1 - \phi_2))}{\tau (\cos(2(\phi_1 - \phi_2)) - 3)}. \quad (\text{A30})$$

Based on the analysis carried out above on a single chain, we change variables $z_1 := \theta_1 + a_1 i \theta_2$, where $a_1 = \sqrt{(1 + \mu)/(1 - \mu)}$ and $z_2 := \phi_1 + a_2 i \phi_2$, where $a_2 = \sqrt{(3 + \mu - 2\rho)/(-3 - \mu + 4\rho)}$ and then to linear order in μ and $\rho - 1$. Such limits correspond to the vicinity of the bifurcation $\mu \ll 1$ and that the case where the two chains have almost the same elasticity $\rho - 1 \ll 1$. Such hypothesis is not strictly necessary to proceed and does not affect

the spirit of the following derivation, yet it drastically simplifies the algebraic manipulations. As a result, we obtain the two coupled ODEs:

$$\dot{z}_1 = (i + \mu)z_1 + \left(-1 - \frac{\mu}{2} + i\left(-\frac{1}{8} + \frac{5}{4}\mu\right)\right)|z_1|^2 z_1 + \frac{\kappa}{2}(i(\mu + 1) - 1)(z_1 + z_1^\dagger - z_2 + z_2^\dagger) \quad (\text{A31})$$

$$\begin{aligned} \dot{z}_2 = & (i(3\mu\rho - 3\mu + \rho) + \mu - 3\rho + 3)z_2 + \left(\frac{i}{8}(-9\mu\rho + 19\mu - 31\rho + 30) - 3\mu\rho + \frac{5\mu}{2} + \frac{\rho}{2} - \frac{3}{2}\right)|z_2|^2 z_2 \\ & + \frac{\kappa}{2}(i(-4\mu\rho + 5\mu - 3\rho + 4) - 1)(z_2 + z_2^\dagger - z_1 + z_1^\dagger) \end{aligned} \quad (\text{A32})$$

These two coupled ODEs represent two coupled oscillators close to a Hopf bifurcation. To proceed further, we assume that the coupling between the chains $\kappa \ll 1$. We can then study the coupling as a perturbation about the two limit cycles of the two elasto-active chains [36]. This hypothesis relies on the assumption that the coupling does not affect the magnitude the self-oscillations, but that it affect their phase. In other words, if we introduce the amplitude and phase of the complex variables z_1 and z_2 by introducing the following variable changes $z_1 = R_1 e^{i\Phi_1}$ and $z_2 = R_2 e^{i\Phi_2}$, the amplitudes will be given by the uncoupled chains and with remain constant $R_1 = \sqrt{\mu}$ and $R_2 = \sqrt{\mu - 3(\rho - 1)}$, and the time-evolution of the phases will be given by the following equations

$$\frac{d\Phi_1}{dt} = 1 - \frac{\mu}{8} + \frac{\kappa}{2} \left[1 + \frac{\sqrt{\mu - 3\rho + 3}}{\sqrt{\mu}} (\sin(\Phi_2 - \Phi_1) - \cos(\Phi_2 - \Phi_1)) \right] \quad (\text{A33})$$

$$\frac{d\Phi_2}{dt} = 1 - \frac{1}{8}(\mu + 11(1 - \rho)) + \frac{\kappa}{2} \left[1 - \frac{\sqrt{\mu}}{\sqrt{\mu - 3\rho + 3}} (\sin(\Phi_1 - \Phi_2) - \cos(\Phi_1 - \Phi_2)) \right], \quad (\text{A34})$$

which is linearized with respect to μ , $\rho - 1$ and κ and where the non-resonant terms proportional to $\sin(2\Phi_1)$, $\sin(2\Phi_2)$ and $\sin(\Phi_1 + \Phi_2)$, on the right-hand side have been neglected. Such terms typically average out and do not contribute to changing the relative phase between the two oscillators $\Phi_1 + \Phi_2$ [36]. Finally, we can subtract the last two equations to express the equation governing the time-evolution of the instantaneous phase difference between the two chains $\Psi := \Phi_2 - \Phi_1$ to obtain

$$\frac{d\Psi}{dt} = d\nu + \varepsilon(\sin \Psi + \tan \Psi_0 \cos \Psi), \quad (\text{A35})$$

where $d\nu := \frac{11}{8}(\rho - 1)$, $\varepsilon := \frac{\kappa(2\mu - 3\rho + 3)}{2\sqrt{\mu}\sqrt{\mu - 3\rho + 3}}$ and $\tan \Psi_0 := \frac{3(\rho - 1)}{2\mu - 3\rho + 3}$. This equation can be recast as

$$\frac{d\Psi}{dt} = d\nu + \frac{\varepsilon}{\cos \Psi_0} \sin \Psi - \Psi_0, \quad (\text{A36})$$

which is a standard equation for non-isosynchronous synchronization [36]. The synchronization occurs when $|d\nu| < |\varepsilon/\cos \Psi_0|$, which, translated in the parameters of the problem, corresponds to coupling constants κ larger than $\kappa_c = 11/(4\sqrt{6})\sqrt{\mu|1 - \rho|}$. Synchronization occurs for vanishingly small coupling close to the bifurcation of the first chain $\mu = 0$ and in the limit where the two chains are identical, that is $\rho = 1$.